AFRL-RI-RS-TR-2024-034

MODEL-BASED AND AI-ASSISTED AUTONOMOUS INTERFERENCE-AVOIDING DIRECTIONAL NETWORKING

FLORIDA ATLANTIC UNIVERSITY

MARCH 2024

FINAL TECHNICAL REPORT

APPROVED FOR PUBLIC RELEASE; DISTRIBUTION UNLIMITED

STINFO COPY

AIR FORCE RESEARCH LABORATORY
INFORMATION DIRECTORATE

■ **AIR FORCE MATERIEL COMMAND** ■ **UNITED STATES AIR FORCE** ■ **ROME, NY 13441**

NOTICE AND SIGNATURE PAGE

Using Government drawings, specifications, or other data included in this document for any purpose other than Government procurement does not in any way obligate the U.S. Government. The fact that the Government formulated or supplied the drawings, specifications, or other data does not license the holder or any other person or corporation; or convey any rights or permission to manufacture, use, or sell any patented invention that may relate to them.

This report is the result of contracted fundamental research deemed exempt from public affairs security and policy review in accordance with SAF/AQR memorandum dated 10 Dec 08 and AFRL/CA policy clarification memorandum dated 16 Jan 09. This report is available to the general public, including foreign nations. Copies may be obtained from the Defense Technical Information Center (DTIC) (http://www.dtic.mil).

AFRL-RI-RS-TR-2024-034 HAS BEEN REVIEWED AND IS APPROVED FOR PUBLICATION IN ACCORDANCE WITH ASSIGNED DISTRIBUTION STATEMENT.

FOR THE CHIEF ENGINEER:

/ S /
ELIZABETH S. BENTLEY, PhD
Work Unit Manager

/ S /
NICK P. KOWALCHUK
RIT Chief Engineer
Computing & Communications Division
Information Directorate

This report is published in the interest of scientific and technical information exchange, and its publication does not constitute the Government's approval or disapproval of its ideas or findings.

REPORT DOCUMENTATION PAGE

1. REPORT DATE	2. REPORT TYPE	3. DATES COVERED	
		START DATE	END DATE
MARCH 2024	FINAL TECHNICAL REPORT	AUGUST 2021	SEPTEMBER 2023

4. TITLE AND SUBTITLE

MODEL-BASED AND AI-ASSISTED AUTONOMOUS INTERFERENCE-AVOIDING DIRECTIONAL NETWORKING

5a. CONTRACT NUMBER	5b. GRANT NUMBER	5c. PROGRAM ELEMENT NUMBER
N/A	FA8750-21-1-0500	62788F

5d. PROJECT NUMBER	5e. TASK NUMBER	5f. WORK UNIT NUMBER
		R36A

6. AUTHOR(S)

Dimitris Pados, George Sklivanitis

7. PERFORMING ORGANIZATION NAME(S) AND ADDRESS(ES)

Florida Atlantic University
777 Glades Road
Boca Raton FL 33431

8. PERFORMING ORGANIZATION REPORT NUMBER

9. SPONSORING/MONITORING AGENCY NAME(S) AND ADDRESS(ES)	10. SPONSOR/MONITOR'S ACRONYM(S)	11. SPONSOR/MONITOR'S REPORT NUMBER(S)
Air Force Research Laboratory/RITGB 525 Brooks Road Rome NY 13441-4505	AFRL/RI	AFRL-RI-RS-TR-2024-034

12. DISTRIBUTION/AVAILABILITY STATEMENT

Approved for Public Release; Distribution Unlimited. This report is the result of contracted fundamental research deemed exempt from public affairs security and policy review in accordance with SAF/AQR memorandum dated 10 Dec 08 and AFRL/CA policy clarification memorandum dated 16 Jan 09.

13. SUPPLEMENTARY NOTES

14. ABSTRACT

We consider the problem of dynamically optimizing a multiple-input multiple-output (MIMO) wireless waveform in a given potentially heavily utilized fixed frequency band with applications in near-field or far-field autonomous machine-to-machine communications. In this report, we cover two novel model-based solutions: (a) Disjoint, space first (transmit weight vector) then time (pulse code sequence) waveform optimization and (b) jointly optimal transmit weight vector and pulse code sequence optimization (a mixed integer programming problem.) The proposed formally derived algorithmic solutions are studied in extensive simulations. The report also covers the evaluation of the proposed algorithms on RF System-on-a-Chip hardware.

15. SUBJECT TERMS

Self-optimized space-time MIMO antijam waveforms, software-programmable networking, reconfigurable ultra-wideband (all-spectrum) RF System-on-a-Chip hardware.

16. SECURITY CLASSIFICATION OF:			17. LIMITATION OF ABSTRACT	18. NUMBER OF PAGES
a. REPORT	b. ABSTRACT	C. THIS PAGE		
U	U	U	SAR	31

19a. NAME OF RESPONSIBLE PERSON	19b. PHONE NUMBER *(Include area code)*
ELIZABETH S. BENTLEY	N/A

PREVIOUS EDITION IS OBSOLETE.

Table of Contents

List of Figures

1 Summary

1.1 Overview and Main Results

The report describes work performed from 09-08-2021 to 30-09-2023 under AFRL grant number FA8750-21-1-0500 entitled "Model-Based and AI-Assisted Autonomous Interference-Avoiding Directional Networking". In contested and degraded electromagnetic environments that extend to hundreds of miles, U.S. Air Force and other Department of Defense personnel and assets deployed on land, air, and space must be capable of maintaining operational wireless connectivity at all times within the laws of physics and hardware limitations. Directional connectivity of tactical networks not only enables effective and efficient use of the available space-time-frequency continuum but also safeguards signals from would-be eavesdroppers. The objective of this effort is to develop and implement model-based and AI-assisted joint space-time waveform design algorithms for directional connectivity of multiple input multiple output (MIMO) network nodes that will enable resilient, self-sustained directional wireless networking of distributed ground/air assets that operate at maximum throughput. We consider the problem of dynamically optimizing a multiple-input multiple-output (MIMO) wireless waveform in a given potentially heavily utilized fixed frequency band width applications in near-field or far-field autonomous machine-to-machine communications. In particular, we find the transmitter beam weight vector and the pulse code sequence that maximize the signal-to-interference-plus-noise ratio (SINR) at the output of the maximum SINR joint space-time receiver filter. We propose and derive two novel model-based solutions: (a) Disjoint, space first (transmit weight vector) then time (pulse code sequence) waveform optimization and (b) jointly optimal transmit weight vector and pulse code sequence optimization (a mixed integer programming problem.) The proposed formally derived algorithmic solutions are studied in extensive simulations under varying waveform code length, near-field/far-field and spread-spectrum/non-spread-spectrum interference, in light and dense interference scenarios. Our findings highlight the effectiveness of the described methods compared to static conventionally designed MIMO links and the remarkable ability of the joint space-time optimized waveforms to avoid heavy interference. Our contributions can be summarized as follows:

- We propose two novel closed loops transmit space-time signal design solutions to dynamically maximize the SINR at the output of the receiver's space-time matched filter for any locally sensed space-time disturbance autocorrelation matrix. The first solution involves searching for an optimized transmitter beam weight vector and separate a posteriori optimization of a digital wave shape code. The second solution involves jointly optimizing the transmitter beam weights and the code vector at increased computational complexity (a mixed integer programming problem.)

- Extensive simulations are carried out to evaluate and compare the effectiveness of the proposed methods under various interference scenarios, including near-field and far-field, spread-spectrum and non-spread-spectrum interference, in light and dense disturbance scenarios. The simulation studies consider varying transmit beam vector and waveform code length and demonstrate the potential of these near/far-field agnostic schemes to dynamically support MIMO links in extreme interference environments.

- We present a 4x4 multi-antenna link implemented on the field-programmable-gate-array (FPGA) fabric of the AMD/Xilinx Zynq Ultrascale RFSoC ZCU111 evaluation board to

demonstrate dynamic interference avoidance in the presence of either narrowband or wideband co-channel interferers. We demonstrate two modes of operation for the link of interest: (i) beamforming mode with beam steering at Tx and conventional/adaptive null-steering beamformer at Rx, and (ii) diversity mode with no beamforming at either side of the link.

The introduction to the project is given in Section 2. Section 3 presents the MIMO system model and notation. Section 4 describes the sensing and waveform optimization problem. Section 5 provides space-time waveform designs with the implementation of a disjoint space-first, time-next optimization method and a joint optimization method. Section 6 provides simulation studies and comparisons. Section 7 presents a 4x4 multi-antenna link implemented on the FPGA fabric of the AMD/Xilinx Zynq Ultrascale RFSoC ZCU111 evaluation board to demonstrate dynamic interference avoidance. A few concluding remarks are drawn in Section 8. Appendix A offers a proof for the closed-form solution of the optimal beam weight vector for any fixed code vector.

1.2 List of People Involved

There are two faculty members involved in the project, which are listed in the following:

- Prof. Dimitris Pados; Florida Atlantic University, PI
- Prof. George Sklivanitis; Florida Atlantic University, Co-PI

Additionally, the project supported one Ph.D. student, working in the project toward her Ph.D. degree, and one postdoctoral research scientist.

1.3 List of Publications

Peer-Reviewed Journal Articles:

- S. Naderi, D. A. Pados, G. Sklivanitis, E. S. Bentley, J. Suprenant and M. J. Medley, "Self-optimizing Near and Far-Field MIMO Transmit Waveforms" to *appear in IEEE JSAC Special Issue on Electromagnetic Signal and Information Theory for Communications, 2024.*

Peer-Reviewed Conference Proceeding Papers:

- S. Naderi, D. A. Pados, G. Sklivanitis, E. S. Bentley, J. Suprenant and M. J. Medley, "Dynamic Interference-Avoiding MIMO Links," *MILCOM 2023 - 2023 IEEE Military Communications Conference (MILCOM)*, Boston, MA, USA, 2023, pp. 827-832, doi: 10.1109/MILCOM58377.2023.10356343.
- A. Torabi, G. Sklivanitis, D. A. Pados, E. S. Bentley, J. Suprenant and M. J. Medley, "Interference-Avoiding RFSoC-based MIMO Links," *MILCOM 2023 - 2023 IEEE Military Communications Conference (MILCOM)*, Boston, MA, USA, 2023, pp. 249-250, doi: 10.1109/MILCOM58377.2023.10356365.

2 Introduction

Interference has always been a crucial concern across all generations of wireless communication systems [1]. Today, given the explosive growth in the number of wireless users and the expectation

of data transfer rates in the order of hundreds of Mbps, especially for emerging technologies such as machine-to-machine communications [2]-[4], broadband Internet of Things [5], millimeter wave (mm-wave) robotics [4], wireless security [6]-[8], ultra-reliable low latency (URLLC) networks [9], enhanced mobile broadband (eMBB) [10], massive machine-type communications (mMTC) [11], etc., interference management and avoidance become increasingly challenging and attract significant attention [1], [12], [13]. A method to deal with interference concerns is interference avoidance via dynamic waveform design at a fine time scale [14]-[18] where a finite sequence of repeated pulses (say, square-root-raised cosines (SRRC)) that span the entire continuum of the device-accessible spectrum is code optimized over a finite pulse-modulation alphabet to maximize the signal-to-interference-plus-noise ratio (SINR) at the output of the max-SINR filter at the intended receiving node [19], [20].

Multiple-input multiple-output (MIMO) technology is by now well understood as a crucial component in 5G and beyond communications [21]-[23]. MIMO systems increase channel capacity, reduce bit-error-rate (BER) and power consumption for a fixed channel data rate, and present unique interference avoidance opportunities in the form of directional transmission and space-time precoding and directional reception and space-time filtering that exploit the product of the spatial and time domain degrees of freedom (DOF) [24], [25]. There are on-going efforts in the literature to deal with interference dilemmas in the time domain by deploying distributed deep learning models, such as [26] that considered 5G/broadband IoT networks. In [20], a similar IoT network was considered but instead of deep learning, an optimal adaptive sparse waveform design algorithm was proposed which adjusts digitally the shape of the waveforms in such a way that the SINR at the output of the maximum-SINR linear filter at the receiver was maximized. A mechanism for interference management in MIMO systems was proposed in [27] where the authors focused on the energy loss problem at downlink transmitters and combined power water-filling algorithms with linear precoding to mitigate interference effects between users. In [19], the problem of directional space-time waveform design for proactive interference avoidance in narrowband far-field MIMO systems was considered. The authors proposed to establish communication between an intended transmitter-receiver pair by a jointly optimized pulse code sequence and signal angle-of-arrival (AoA) that maximized the maximum achievable pre-detection SINR at the output of the max-SINR receiver filter. Gaussian MIMO channels under total transmit and interference power constraints were considered in [28], [29] where the authors obtained by the Karush–Kuhn–Tucker (KKT) approach a closed-form solution for the optimal transmit covariance matrix. The work in [30] focused on the weighted sum-rate maximization problem for wireless cellular MIMO networks with full-duplex base stations and half-duplex mobile devices. In this context, an interference shaping algorithm was developed to decompose the sum-rate problem into independent sub-problems solved locally for each base station under varying constraints. A MIMO relay system was considered in [31] where multiple transmitter and receiver pairs communicate at once through a single relay node. For this system model, the authors proposed a new algorithm that jointly optimized the relay precoding matrix and the receiver matrices based on the minimum sum mean-squared error criterion.

In this project, we address for the first time in the literature the challenge of establishing an optimally interference-avoiding near-field MIMO wireless link, targeting for example modern connected robotics applications in high frequency bands (i.e., mm-wave or terahertz (THz).) We recall that near-field effects, which make conventional directional array-response modeling non-applicable, are extended considerably when the diameter of focused antennas exceeds half the wavelength of the

carrier or as the carrier wavelength decreases. As a measure of the interference experienced by an activated MIMO link in the near or far-field, we utilize the conventional SINR metric which is independent of information symbol alphabet specifics. Specifically, we investigate the optimization of the transmitter beam weight vector and the time-domain wave shaping code to maximize the pre-detection SINR at the output of the joint space-time receiver filter for any locally sensed space-time disturbance autocorrelation matrix. We propose two new model-based solutions: (a) A disjoint approach that first optimizes the transmitter beam weight vector and then shapes a digitally coded waveform occupying the entire device accessible frequency band and (b) an optimization approach where the transmitter beam weight vector and the digitally coded waveform are jointly optimized. Our contributions can be summarized as follows:

- We propose two novel closed loops transmit space-time signal design solutions to dynamically maximize the SINR at the output of the receiver's space-time matched filter for any locally sensed space-time disturbance autocorrelation matrix. The first solution involves searching for an optimized transmitter beam weight vector and separate a posteriori optimization of a digital wave shape code. The second solution involves jointly optimizing the transmitter beam weights and the code vector at increased computational complexity (a mixed integer programming problem.)

- Extensive simulations are carried out to evaluate and compare the effectiveness of the proposed methods under various interference scenarios, including near-field and far-field, spread-spectrum, and non-spread-spectrum interference, in light and dense disturbance scenarios. The simulation studies consider varying transmit beam vector and waveform code length and demonstrate the potential of these near/far-field agnostic schemes to dynamically support MIMO links in extreme interference environments.

Notation: Matrices are denoted by upper-case bold letters, column vectors by lower-case bold letters, and scalars by lower-case plain-font letters. The transpose operation is represented by the superscript ^{T}, conjugation by *, the Hermitian operation (conjugate transpose) by ^{H}, and the Kronecker product by $\otimes$.

3 Methods, Assumptions and Procedures

We consider an arbitrary multi-antenna (MIMO) link configuration with M_t transmit and M_r receive antennas as seen in Fig. 1. Without loss of generality, we assume that the transmitter sends an information bit sequence $b(n) \in \{\pm 1\}$, $n = 0,1,\dots,N$, at rate $1/T_b$ *across all antennas* on a carrier frequency f_c using an underlying digitally shaped waveform $s(t)$ of duration T_b. Specifically, the signal transmitted by the m_tth transmit antenna, $m_t = 1,2,\dots,M_t$, is represented by

$$x_{m_t}(t) = \sqrt{E_t}\sum_{n=0}^{N-1} b\,(n)s(t - nT_b)e^{j2\pi f_c t}w_{m_t} \qquad (1)$$

where E_t is the transmitted energy per bit per antenna, $w_{m_t} \in \mathbb{C}$ is the complex antenna beam weight parameter and the digitally pulse-coded waveform $s(t)$ is given by

$$s(t) = \sum_{l=0}^{L-1} s\,(l) p_{T_c}(t - lT_c) \qquad (2)$$

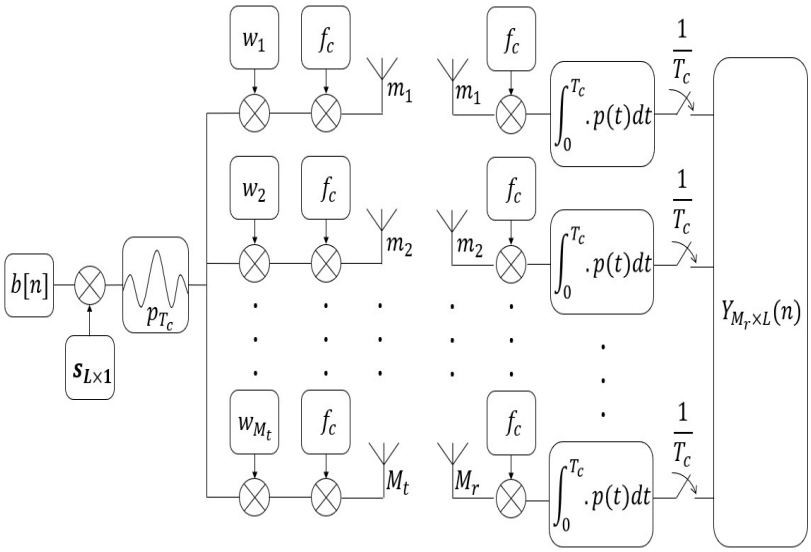

Figure 1: MIMO system model.

where $\mathbf{s}(\mathrm{l}) \in \{\pm 1/\sqrt{L}\}$ is the l th code bit of the code vector $\boldsymbol{s}_{Lx1}$, and $p_{T_c}(.)$ is a square-root raised cosine (SRRC) pulse with roll-off factor α and duration T_c where $T_b = LT_c$ and the bandwidth of the transmitted signal is $\beta = (1+\alpha)/T_c$. For clarity in presentation, it is assumed that the individual pulses are normalized to unit energy

$$\int_0^{T_c} |p_{Tc}(t)|^2\, dt = 1. \qquad (3)$$

The receiver consists of M_r antenna elements. After carrier demodulation of the transmitted signal, the receiving antennas capture

$$\mathbf{r}_{M_r\times 1}(t) = \sqrt{E_t} \sum_{n=0}^{N-1} b\,(n) s(t - nT_b)\mathbf{H}^T \mathbf{w}_{M_t} + \mathrm{i}(t) + \mathbf{n}(t) \qquad (4)$$

where $\mathbf{H} \in \mathbb{C}^{M_t \times M_r}$ is a generic channel matrix assumed to remain constant over NT_b sec,

$$\mathbf{H} \triangleq \begin{bmatrix} h_{1,1} & h_{1,2} & \dots & h_{1,M_r} \\ h_{2,1} & h_{2,2} & \dots & h_{2,M_r} \\ \vdots & \vdots & \ddots & \vdots \\ h_{M_t,1} & h_{M_t,2} & \dots & h_{M_t,M_r} \end{bmatrix} \qquad (5)$$

where $h_{m_t,m_r} \in \mathbb{C}$ is the complex coefficient of the channel between the m_tth transmit antenna and the m_rth receive antenna. We recall that if two transmit antennas $m_t = i, j$ are in the far-field of a

receive antenna $m_r = k$, then $h_{i,k}$ and $h_{j,k}$ have approximately equal phase (and amplitude), which enables effective directional signal reception by an appropriately set receiver array. Instead, if the two transmit antennas $m_t = i, j$ are in the near field of $m_r = k$, then the phase of $h_{i,k}$ and $h_{j,k}$ vary significantly. Conventionally, we set the beginnings of the far field at the distance at which the experienced phase difference is less than $\pi/8$ (Fraunhofer distance) [32]. Returning to the description of (4), $\mathbf{w}_{M_t} \in \mathbb{C}^{M_t}$ is the transmitter beam weight vector, $\mathbf{n}(t) \in \mathbb{C}^{M_r \times 1}$ denotes a complex Gaussian noise process that is assumed white both in time and space, and $\mathbf{i}(t) \in \mathbb{C}^{M_r}$ models comprehensively environmental disturbance of any other form.

For a given fixed bit period n, $n = 1,2,\ldots,N$, upon pulse matched-filtering and sampling over L pulses at each receive antenna element, the collected values are organized in the form of a space-time data matrix $\mathbf{Y}_{M_r x L}(n)$ (see Fig. 1). The data matrix is then vectorized to

$$\begin{aligned} \mathbf{y}_{M_r L \times 1}(n) = Vec\{\mathbf{Y}_{M_r \times L}(n)\} = \\ = \sqrt{E_t} b(n)(\mathbf{s} \otimes \mathbf{H}^T)\mathbf{w}_{M_t} + \mathbf{i}(n) + \mathbf{n}(n) \end{aligned} \quad (6)$$

where $\mathbf{i}(n)$ and $\mathbf{n}(n)$ represent post pulse-matched-filtering interference and white noise in the space-time receiver domain. In the following section, we derive the maximum-SINR optimal joint space-time receiver filter in the $M_r L$ product vector space and we find its output SINR as a function of $\mathbf{s}$ (time-domain code) and $\mathbf{w}_{M_t}$ (transmit beam vector), creating therefore the foundation for space and time transmit waveform optimization (closed-loop interference avoiding space and time precoding.)

4 Sensing and Waveform Optimization Problem

For the given received space-time data vector in (6), the space-time receiver matched filter (MF) is by definition given by

$$\mathbf{w}_{\mathrm{MF}} \triangleq E\{\mathbf{y}_{M_r L \times 1}(n)\ b(n)\} = (\mathbf{s} \otimes \mathbf{H}^T)\mathbf{w}_{M_t}. \quad (7)$$

The compound space-time disturbance $\mathbf{i}(n) + \mathbf{n}(n)$, assumed to be zero mean for simplicity, has autocorrelation/autocovariance matrix defined by

$$\mathbf{R}_{i+n} \triangleq E\left\{\big(\mathbf{i}(n) + \mathbf{n}(n)\big)\big(\mathbf{i}(n) + \mathbf{n}(n)\big)^H\right\} \in \mathbb{C}^{M_r L \times M_r L}. \quad (8)$$

In view of (7) and (8), the space-time maximum SINR receiver filter becomes

$$\mathbf{w}_{\max-\mathrm{SINR}} = k\,\mathbf{R}_{i+n}^{-1}(\mathbf{s} \otimes \mathbf{H}^T)\mathbf{w}_{M_t},\ k \in \mathbb{C}. \quad (9)$$

We can now calculate the output SINR of the maximum SINR space-time receiver filter as follows,

$$\mathrm{SINR}\big(\mathbf{s}, \mathbf{w}_{M_t}\big) \triangleq \frac{\mathrm{E}\left\{\left|\mathbf{w}_{\max-\mathrm{SINR}}^H\big(\sqrt{E_t} b(n)(\mathbf{s} \otimes \mathbf{H}^T)\mathbf{w}_{M_t}\big)\right|^2\right\}}{\mathrm{E}\left\{\left|\mathbf{w}_{\max-\mathrm{SINR}}^H\big(\mathbf{i}(n) + \mathbf{n}(n)\big)\right|^2\right\}}$$

$$= E_t\big[(\mathbf{s} \otimes \mathbf{H}^T)\mathbf{w}_{M_t}\big]^H \mathbf{R}_{i+n}^{-1}(\mathbf{s} \otimes \mathbf{H}^T)\mathbf{w}_{M_t}. \quad (10)$$

We see, therefore, that the SINR at the output of the maximum SINR space-time receiver filter for the general near-field MIMO link model under examination is a closed form expression of the transmit beam weight vector $\mathbf{w}_{M_t} \in \mathbb{C}^{M_t}$ and the time domain code vector $\mathbf{s} \in \{\pm 1/\sqrt{L}\}^L$. It is of interest, then, to investigate what waveform design values $\mathbf{w}_{M_t}$ and $\mathbf{s}$ maximize the maximum attainable SINR by the receiver filter for a locally sensed space-time disturbance-only autocorrelation matrix

$$\widehat{\mathbf{R}}_{i+n} = \sum_{k=1}^{K} \big(\mathbf{i}(k) + \mathbf{n}(k)\big)\big(\mathbf{i}(k) + \mathbf{n}(k)\big)^H \quad (11)$$

over K samples and estimated MIMO channel state information matrix $\mathbf{H}$.

In the following section, we present two distinct space-time waveform design methods.

5 Space-Time Waveform Design

In this section, we develop and describe in implementation detail two space-time waveform design methods. The first method carries out disjoint space-first, time-next optimization, i.e., we first suggest an optimized transmit beam weight vector $\mathbf{w}_{M_t}$ and then find the conditionally optimal code vector $\mathbf{s}$ given $\mathbf{w}_{M_t}$. The second method that we present produces a jointly optimal ($\mathbf{w}_{M_t}$, $\mathbf{s}$) pair.

5.1 Disjoint space and time optimization

We concentrate first in the space domain operation. Considering only the lth column of the data matrix $\mathbf{Y}_{M_r x L}(n)$ in Fig. 1 and following the notation in (4), we have

$$\mathbf{y}_l(n) = \sqrt{E_t} b(n) s(l) \mathbf{H}^T \mathbf{w}_{M_t} + \mathbf{i}(l,n) + \mathbf{n}(l,n) \in \mathbb{C}^{M_r}, \quad (12)$$

$l \in \{1,2,\ldots,L\}$, $n \in \{1,2,\ldots,N\}$. The space-only disturbance autocorrelation matrix is defined by

$$\mathbf{R}_{i+n}^{s} \triangleq E\left\{\big(\mathbf{i}(l,n) + \mathbf{n}(l,n)\big)\big(\mathbf{i}(l,n) + \mathbf{n}(l,n)\big)^H\right\} \in \mathbb{C}^{M_r \times M_r};$$

the space-only maximum SINR filter is

$$\mathbf{w}_{\max-\mathrm{SINR}} = k\, \mathbf{R}_{i+n}^{s^{-1}} \mathbf{H}^T \mathbf{w}_{M_t} \in \mathbb{C}^{M_r},\ k \in \mathbb{C}; \quad (14)$$

and its output SINR is

$$\mathrm{SINR}\big(\mathbf{w}_{M_t}\big) = E_t \big(\mathbf{H}^T \mathbf{w}_{M_t}\big)^H \mathbf{R}_{i+n}^{s^{-1}} \big(\mathbf{H}^T \mathbf{w}_{M_t}\big). \quad (15)$$

By (15) (a quadratic expression in $\mathbf{H}^T \mathbf{w}_{M_t}$), we recognize that if $\mathbf{q}_{space} \in \mathbb{C}^{M_r}$ is the maximum-eigenvalue eigenvector of the space domain inverse disturbance autocorrelation matrix $\mathbf{R}_{i+n}^{s^{-1}}$, then the maximum SINR optimal beam weight vector $\mathbf{w}_{M_t}^{opt}$ is such that

$$\mathbf{H}^T \mathbf{w}_{M_t}^{opt} = \mathbf{q}_{space}. \quad (16)$$

If $M_t = M_r$ and $\mathbf{H} \in \mathbb{C}^{(M_t=M_r)\times(M_t=M_r)}$ is full rank, then

$$\mathbf{w}_{M_t}^{opt} = inv(\mathbf{H}^T)\mathbf{q}_{space}. \qquad (17)$$

If $M_t \neq M_r$ and $\mathbf{H}\mathbf{H}^T$ is full rank (i.e., $M_t < M_r$), then we calculate

$$\mathbf{w}_{M_t}^{opt} = inv(\mathbf{H}\mathbf{H}^T)\mathbf{H}\mathbf{q}_{space}. \qquad (18)$$

The next step is to search for a binary antipodal code sequence $\mathbf{s} \in \{\pm 1/\sqrt{L}\}^L$ so that the corresponding final space-time post-filtering SINR$\left(\mathbf{s}, \mathbf{w}_{M_t}^{opt}\right)$ is maximized. Utilizing (10) for fixed $\mathbf{w}_{M_t} = \mathbf{w}_{M_t}^{opt}$, the remaining optimization problem can be written as

$$\mathbf{s}^{\text{opt}} = \underset{\mathbf{s}\in\{\pm 1/\sqrt{L}\}^L}{\text{argmax}} \left\{ \left[(\mathbf{s} \otimes \mathbf{H}^T)\mathbf{w}_{M_t}^{opt}\right]^H \mathbf{R}_{i+n}^{-1} (\mathbf{s} \otimes \mathbf{H}^T)\mathbf{w}_{M_t}^{opt} \right\} \qquad (19)$$

where $\mathbf{R}_{i+n} \in \mathbb{C}^{M_r L \times M_r L}$ is the joint space-time disturbance autocorrelation matrix defined by (8). An optimized code sequence for the given $\mathbf{w}_{M_t}^{opt}$ transmit beam vector can be found by a one-dimensional search over 2^L candidate code sequences. The complete disjoint space and time optimization algorithm is summarized in Fig. 2 for easy reference. Its overall computational complexity is $\mathcal{O}(2M_t^3 + (M_r L)^3 + 4M_t M_r L + 4M_t M_r + 2^{L-1})$ (the code-vector quadratic optimization sub-problem is sign insensitive.)

The separately optimized code and transmit beam weight vectors $\mathbf{s}^{opt}, \mathbf{w}_{M_t}^{opt}$ define the interference-avoiding MIMO link waveform. Under the assumption that $\mathbf{s}^{opt}, \mathbf{w}_{M_t}^{opt}$ are made available to the transmitter within the $\mathbf{H}$ and $\mathbf{R}_{i+n}$ channel coherence time, the output SINR of the joint space-time

Algorithm 1: Disjoint space and time optimization

Input: Pulse-filtered interference-plus-noise received samples;
estimated channel matrix $\mathbf{H} \in \mathbb{C}^{M_t \times M_r}$.

1: Calculate (estimate) space-only disturbance autocorrelation matrix $\mathbf{R}_{\mathbf{i+n}}^{\mathbf{s}} \in \mathbb{C}^{M_r \times M_r}$ in (13).

2: Calculate minimum-eigenvalue eigenvector of $\mathbf{R}_{i+n}^{s}$, $\mathbf{q}_{space} \in \mathbb{C}^{M_r}$.

3: If $M_t = M_r$, $\mathbf{w}_{M_t}^{opt} = inv(\mathbf{H}^T)\mathbf{q}_{space}$.

4: If $M_t \neq M_r$, $\mathbf{w}_{M_t}^{opt} = inv(\mathbf{H}\mathbf{H}^T)\mathbf{H}\mathbf{q}_{space}$.

5: Find optimum code $\mathbf{s}^{opt} \in \{\pm 1/\sqrt{L}\}^L$ (or other alphabet) by discrete search over (19).

Output: $\mathbf{w}_{M_t}^{opt}$, $\mathbf{s}^{\text{opt}}$.

Figure 2: Proposed disjoint first-space, then-time optimization algorithm.

receiver filter is conditionally maximized at operational information rate $1/LT_c$ symbols per second where T_c is the duration of the utilized SRRC pulse.

5.2 Joint Space-Time Optimization

We now revisit (10) and attempt to jointly optimize $\mathbf{s}$ and $\mathbf{w}_{M_t}$; that is, we attempt to solve

$$\left(\mathbf{s}^{opt}, \mathbf{w}_{M_t}^{opt}\right) = \underset{\mathbf{s}\in\{\pm 1/\sqrt{L}\}^L, \mathbf{w}_{M_t}\in\mathbb{C}^{M_t}}{\operatorname{argmax}} \left\{\left[(\mathbf{s}\otimes\mathbf{H}^T)\mathbf{w}_{M_t}\right]^H \mathbf{R}_{i+n}^{-1}(\mathbf{s}\otimes\mathbf{H}^T)\mathbf{w}_{M_t}\right\}. \quad (20)$$

From (20), we recognize that -code domain and MIMO channel specifics aside- the overall jointly optimal space-time waveform is the maximum-eigenvalue eigenvector $\mathbf{q}_{\mathrm{s-t}} \in \mathbb{C}^{M_r L}$ of the inverse of the joint space-time disturbance autocorrelation matrix

$$\mathbf{R}_{i+n} \triangleq E\left\{\left(\mathbf{i}(n)+\mathbf{n}(n)\right)\left(\mathbf{i}(n)+\mathbf{n}(n)\right)^H\right\} \in \mathbb{C}^{M_r L\times M_r L}, \quad (21)$$

which coincides with the smallest-eigenvalue eigenvector of $\mathbf{R}_{i+n}$. As an effective surrogate to the mixed-integer optimization problem in (20), we suggest l_2 -norm approximation of $\mathbf{q}_{\mathrm{s-t}}$ by $(\mathbf{s}\otimes\mathbf{H}^T)\mathbf{w}_{M_t}$, i.e., we try to solve

$$\left(\mathbf{s}^{opt}, \mathbf{w}_{M_t}^{opt}\right) = \underset{\mathbf{s}\in\{\pm 1/\sqrt{L}\}^L, \mathbf{w}_{M_t}\in\mathbb{C}^{M_t}}{\operatorname{argmin}} ||\mathbf{q}_{s-t} - (\mathbf{s}\otimes\mathbf{H}^T)\mathbf{w}_{M_t}||^2. \quad (22)$$

We can prove (see Appendix) that a closed-form expression of $\mathbf{w}_{M_t}^{opt}$ for any fixed code vector $\mathbf{s}$ is

$$\mathbf{w}_{M_t}^{opt} = inv[(\mathbf{s}^T\otimes\mathbf{H}^*)(\mathbf{s}\otimes\mathbf{H}^T)](\mathbf{s}^T\otimes\mathbf{H}^*)\mathbf{q}_{s-t} \quad (23)$$

where $(\mathbf{s}^T\otimes\mathbf{H}^*)(\mathbf{s}\otimes\mathbf{H}^T)$ is invertible if $rank(\mathbf{H}) \geq M_t$. Inserting now (23) in (22) (or (20), we can find the jointly optimal code vector $\mathbf{s}^{opt}$ with a simple binary search

$$\mathbf{s}^{opt} = \underset{\mathbf{s}\in\{\pm 1/\sqrt{L}\}^L}{\operatorname{argmin}} ||\mathbf{q}_{s-t} - (\mathbf{s}\otimes\mathbf{H}^T) \quad inv[(\mathbf{s}^T\otimes\mathbf{H}^*)(\mathbf{s}\otimes\mathbf{H}^T)](\mathbf{s}^T\otimes\mathbf{H}^*)\mathbf{q}_{s-t}||^2$$

$$= \underset{\mathbf{s}\in\{\pm 1/\sqrt{L}\}^L}{\operatorname{argmin}} ||\{\mathbf{I} - (\mathbf{s}\otimes\mathbf{H}^T)[(\mathbf{s}^T\otimes\mathbf{H}^*)(\mathbf{s}\otimes\mathbf{H}^T)]^{-1} \quad (\mathbf{s}^T\otimes\mathbf{H}^*)\}\mathbf{q}_{s-t}||^2 \quad (24)$$

where $\mathbf{I}$ is the $M_r L \times M_r L$ identity matrix. Reverting to (23), we calculate $\mathbf{w}_{M_t}^{opt}$. The overall joint space-time optimization algorithm is summarized for easy reference in Fig. 3. The computational complexity is $\mathcal{O}(M_t^3 + M_t^2 + M_t^2 M_r L + 4M_t M_r L + 2^{L-1})$.

It is of interest to mention that to the extent that our joint design of $\mathbf{s}^{opt}$ and $\mathbf{w}_{M_t}^{opt}$ by (22) succeeds in approximating closely the eigenvector $\mathbf{q}_{s-t}$, i.e., $(\mathbf{s}^{opt} \otimes \mathbf{H}^T)\mathbf{w}_{M_t}^{opt} \approx \mathbf{q}_{s-t}$, then $\mathbf{R}_{i+n}^{-1}(\mathbf{s}^{opt} \otimes \mathbf{H}^T)\mathbf{w}_{M_t}^{opt} = c\,(\mathbf{s}^{opt} \otimes \mathbf{H}^T)\mathbf{w}_{M_t}^{opt}$, $c \in \mathbb{C}$. Therefore, the space-time maximum SINR receiver filter $\mathbf{w}_{\max-\mathrm{SINR}} = k\,\mathbf{R}_{i+n}^{-1}(\mathbf{s} \otimes \mathbf{H}^T)\mathbf{w}_{M_t}$, $k \in \mathbb{C}$, degenerates conveniently to the matched-filter (MF) $(\mathbf{s}^{opt} \otimes \mathbf{H}^T)\mathbf{w}_{M_t}^{opt}$. As before, the operational information rate of the link is $1/LT_c$ symbols per second where T_c is the duration of the utilized SRRC pulse.

Algorithm 2: Joint space-time optimization

Input: Pulse-filtered interference-plus-noise received samples; estimated channel matrix $\mathbf{H} \in \mathbb{C}^{M_t \times M_r}$.

1: Calculate (estimate) space-time disturbance autocorrelation matrix $\mathbf{R}_{i+n} \in \mathbb{C}^{M_r L \times M_r L}$ in (21).

2: Calculate minimum-eigenvalue eigenvector of $\mathbf{R}_{i+n}$, $\mathbf{q}_{s-t} \in \mathbb{C}^{M_r L}$.

3: Find optimum code $\mathrm{s}^{opt} \in \{\pm 1/\sqrt{L}\}^L$ (or other alphabet) by discrete search over (24).

4: Find jointly optimal beam weight vector $\mathrm{w}_{M_t}^{opt}$ by inserting s^{opt} in (23).

Output: $\mathrm{w}_{M_t}^{opt}$, $\mathrm{s}^{\mathrm{opt}}$.

Figure 3: Proposed joint space-time optimization algorithm.

6 Results and Discussions

This section presents simulation results that demonstrate the effectiveness of the proposed formal MIMO waveform optimization methods using as direct performance evaluation metric the SINR at the output of the maximum-SINR space-time receiver filter. To model disturbance effects, we consider near-field/far-field and spread-spectrum/non-spread-spectrum interference signals in all four possible combinations. We evaluate the performance of the proposed waveforms in light and dense interference, where in the light interference scenario we assume there are $M_r/2$ interfering transmitters of each interference type and in the dense interference scenario $5M_r$ interfering transmitters of each interference type. In all studies, the data record size used to estimate the disturbance autocorrelation matrix needed for the computation of $\mathbf{w}_{M_t}^{opt}$ and $\mathbf{s}^{\mathrm{opt}}$ by Fig. 2 or Fig. 3 and the computation of $\mathbf{w}_{\max-\mathrm{SINR}}$ by (9) is set to $N = 100$. All presented results are averages over 10000 independent experiments.

In particular, near-field non-spread-spectrum interfering signals are described by

$$\mathbf{i}_1(t) = \sqrt{E_1} \sum_n b_1[n]\,p(t - nT_b)\mathbf{H}_1^T\mathbf{w}_{M_{t_1}}, \qquad (25)$$

with bandwidth $\frac{1}{T_b}$, $\mathbf{w}_{M_{t_1}}$ transmit antennas, $b_1[n] \in \{\pm 1\}$, and $\mathbf{H}_1 \in \mathbb{C}^{M_{t_1} \times M_r}$.

Near-field spread-spectrum interfering signals are described by

$$\mathbf{i}_2(t) = \sqrt{E_2} \sum_n b_2[n] s_2(t - nT_b) \mathbf{H}_2^T \mathbf{w}_{M_{t_2}}, \qquad (26)$$

$$\mathbf{s}_2(t) = \sum_{l=0}^{L-1} \mathbf{s}_2(l) p_{T_c}(t - lT_c), \qquad (27)$$

with bandwidth $\frac{L}{T_b}$, $\mathbf{s}_2(l) \in \{\pm 1/\sqrt{L}\}$, $\mathbf{w}_{M_{t_2}}$ transmit antennas, $b_2[n] \in \{\pm 1\}$, and $\mathbf{H}_2 \in \mathbb{C}^{M_{t_2} \times M_r}$.

Far-field interfering signals have a directional interference effect on the M_r-element receiver front, which is modeled herein by an array response vector that assumes for simplicity linear uniform geometry and inter-element spacing equal to half the carrier wavelength. In particular, far-field non-spread-spectrum interfering signals are described by

$$\mathbf{i}_3(t) = \sqrt{E_3} \sum_n b_3[n] p(t - nT_b) h_3 \mathbf{a}(\theta_3), \qquad (28)$$

with bandwidth $\frac{1}{T_b}$, $b_3[n] \in \{\pm 1\}$, flat-fading coefficient $h_3 \in \mathbb{C}$, and array response vector $\mathbf{a}(\theta_3) \in \mathbb{C}^{M_r}$ with angle of arrival $\theta_3 \in \left(-\frac{\pi}{2}, \frac{\pi}{2}\right)$. Far-field spread-spectrum interfering signals are described by

$$\mathbf{i}_4(t) = \sqrt{E_4} \sum_n b_4[n] s_4(t - nT_b) h_4 \mathbf{a}(\theta_4), \qquad (29)$$

$$\mathbf{s}_4(t) = \sum_{l=0}^{L-1} \mathbf{s}_4(l) p_{T_c}(t - lT_c), \qquad (30)$$

with bandwidth $\frac{L}{T_b}$, $\mathbf{s}_4(l) \in \{\pm 1/\sqrt{L}\}$, flat-fading coefficient $h_4 \in \mathbb{C}$, and array response vector $\mathbf{a}(\theta_4) \in \mathbb{C}^{M_r}$ with angle of arrival $\theta_4 \in \left(-\frac{\pi}{2}, \frac{\pi}{2}\right)$.

In Fig. 4, we study the pre-detection SINR of a MIMO link with $M_t = M_r = 4$ antennas in light near-field non-spread-spectrum interference under no waveform optimization, code only optimization, transmit beam vector only optimization, disjoint transmit beam vector optimization followed by code vector optimization, and joint beam-code optimization. The number of transmit antennas of each of the $M_r/2 = 2$ interferers is $M_{i_1} = 4$ and their energy-per-bit-over-N_0 value per antenna is set at $10dB$ where $N_0/2$ denotes the power spectral density of the underlying Gaussian vector noise process assumed to be white across time and space (antenna points). Fig. 4(a) assumes codelength $L = 4$ and Fig. 4(b) assumes codelength $L = 16$. Figs. 5(a) and 5(b) repeat the same studies for dense near-field non-spread-spectrum interference (i.e., $5M_r = 20$ interferers) with energy-per-bit-over-N_0 value per antenna equal to $15dB$. An overall observation is that the MIMO link easily handles light or dense near-field non-spread-spectrum interference and the joint space-time waveform optimization approach offer $6dB$ or more gain over the disjoint space first, time next optimization approach at any transmit-energy-per-bit per antenna level. For example, a target pre-detection SINR value equal to $15dB$ (practically error-free binary phase-shift-keying decoding) is attained by joint space-time

optimization at about $1/15th$ of the transmit-energy-per-bit per antenna required under disjoint optimization. Comparing against no optimization whatsoever (arbitrary waveform), the fraction becomes $1/35$. Finally, as expected, for large codelengths, beam vector optimization only and beam vector optimization followed by code vector optimization have about the same pre-detection SINR yield (Figs. 4(b) and 5(b).)

Figs. 6 and 7 repeat the studies of Figs. 4 and 5 under the more challenging scenario of spread-spectrum near-field interference with codelengths that follow the codelength of the main link. The trends and gains in favor of joint space-time optimization remain the same, but Fig. 7(a) highlights the difficulty in dealing with dense near-field spread-spectrum disturbance and the importance of having sufficiently large codelength to operate and optimize (Fig. 7(b).)

Figs. 8 and 9 study far-field non-spread-spectrum interference with conclusions similar to the near-field corresponding case (impressive pre-detection SINR gain by the jointly optimized waveform.)

Figs. 10 and 11 study spread-spectrum far-field interference, regarded arguably as a simpler case than its near-field counterpart. Indeed, optimized waveforms handle well dense far-field spread-spectrum interference even with small codelengths (see for example Fig. 11(a).)

Fig. 12 adds up all types of interference in their dense form, that is, twenty near-field and twenty far-field non-spread-spectrum interferers, as well as twenty near-field and twenty far-field spread-spectrum interferers, all at $15dB$ energy-per-bit-over-N_0 value per transmit antenna. Given sufficient degrees of freedom in the time domain, such as $L = 16$ in Fig. 12(b), the two proposed disjointly and jointly optimized MIMO waveforms readily attain $10dB$ and $15dB$ pre-detection SINR, correspondingly.

All studies presented above assumed perfect channel state information, i.e. knowledge of the MIMO channel matrix $\mathbf{H} \in \mathbb{C}^{M_t \times M_r}$ (as well as perfect pulse/symbol synchronization.) Instead, Fig. 13 reproduces the studies of Fig. 12(b) under imperfect channel knowledge with independent zero-mean complex Gaussian error per channel coefficient and mean-square estimation error $\sigma^2 = \epsilon \times 10^{-E_t/N_0(dB)/10}$ where $\epsilon = 5$ is set to represent the level of channel knowledge imperfection in our study . A moderate SINR loss is observed compared to Fig. 12(b) that diminishes as the mean-square error decreases for increasing E_t/N_0 values.

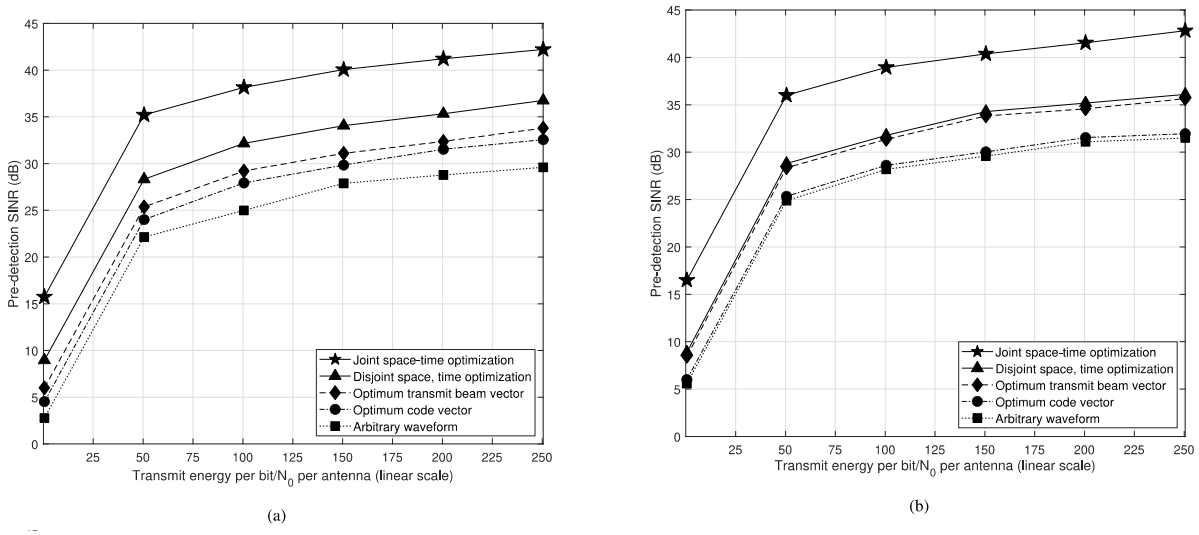

Figure 4: Pre-detection SINR in light near-field non-spread-spectrum interference ($M_t = M_r = M_{i_1} = 4$): (a) L = 4, (b) L = 16.

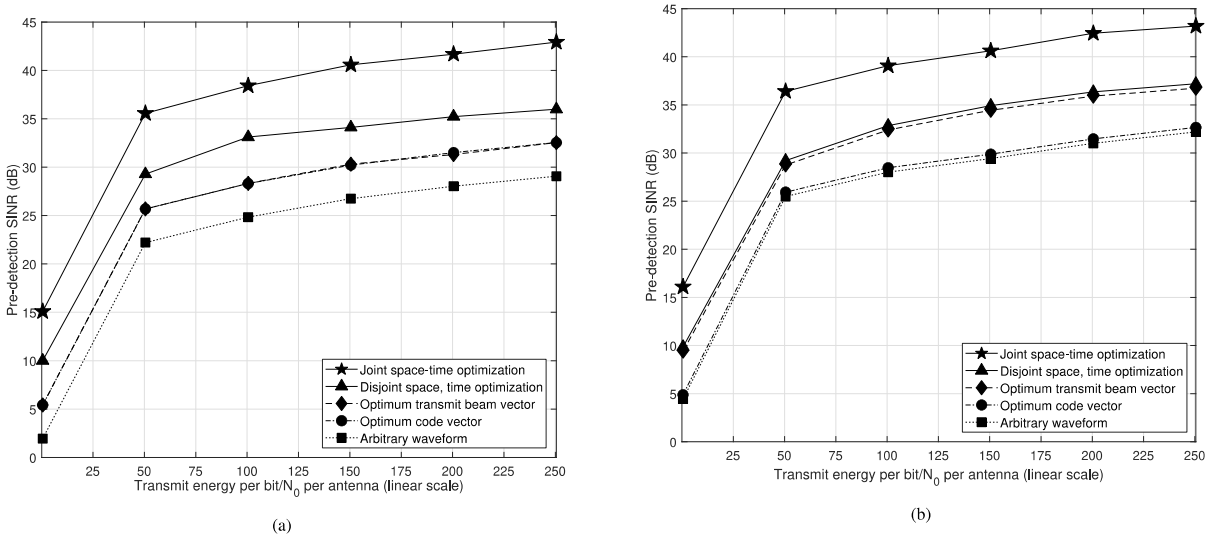

Figure 5: Pre-detection SINR in dense near-field non-spread-spectrum interference ($M_t = M_r = M_{i_1} = 4$): (a) L = 4, (b) L = 16.

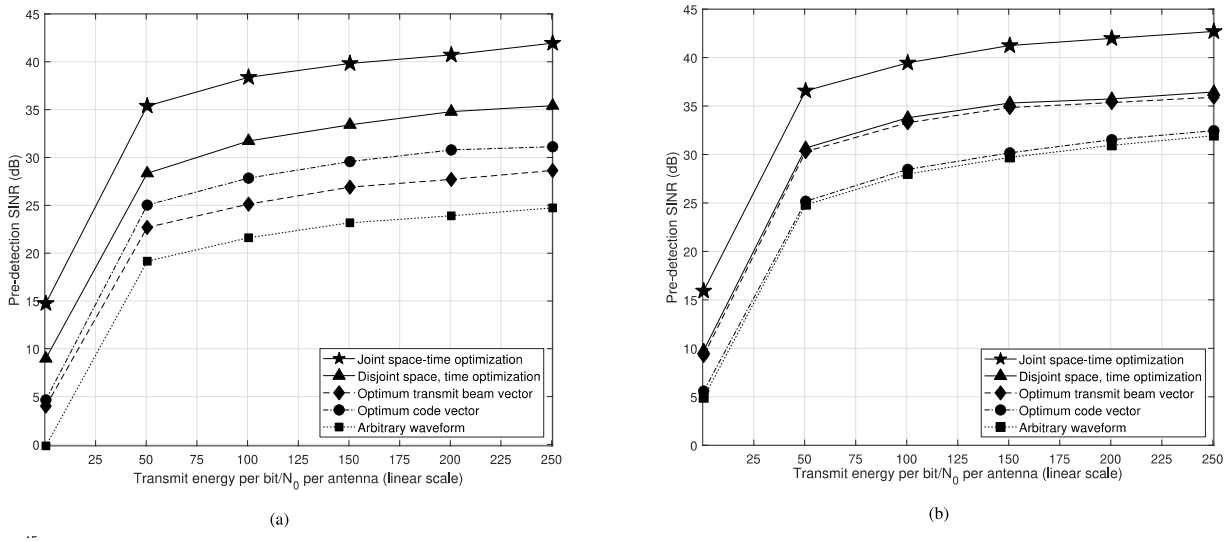

Figure 6: Pre-detection SINR in light near-field spread-spectrum interference (M_t = M_r =M_{i_2} = 4): (a) L = 4, (b) L = 16.

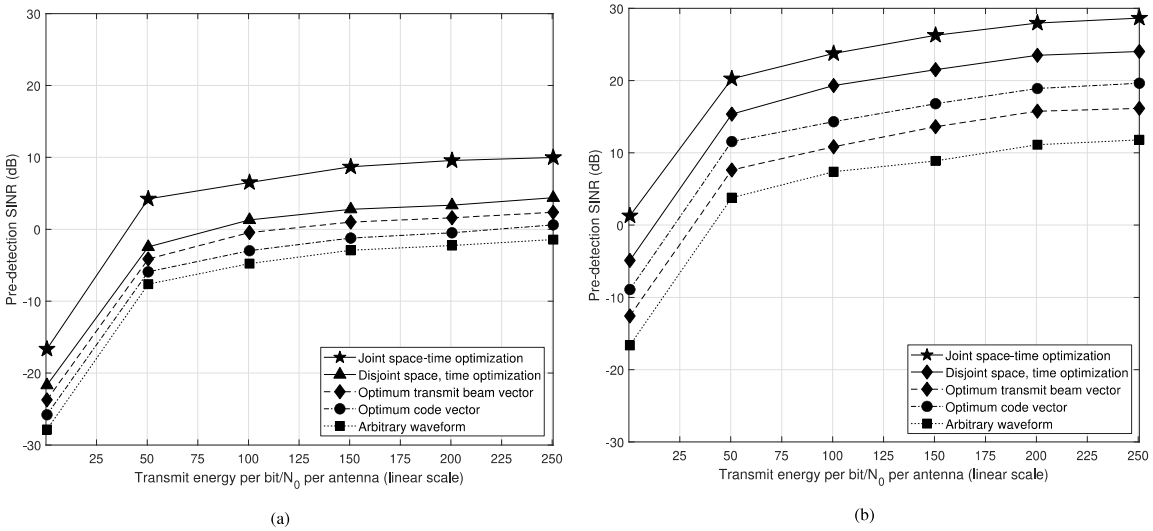

Figure 7: Pre-detection SINR in dense near-field spread-spectrum interference (M_t = M_r =M_{i_2} = 4): (a) L = 4, (b) L = 16.

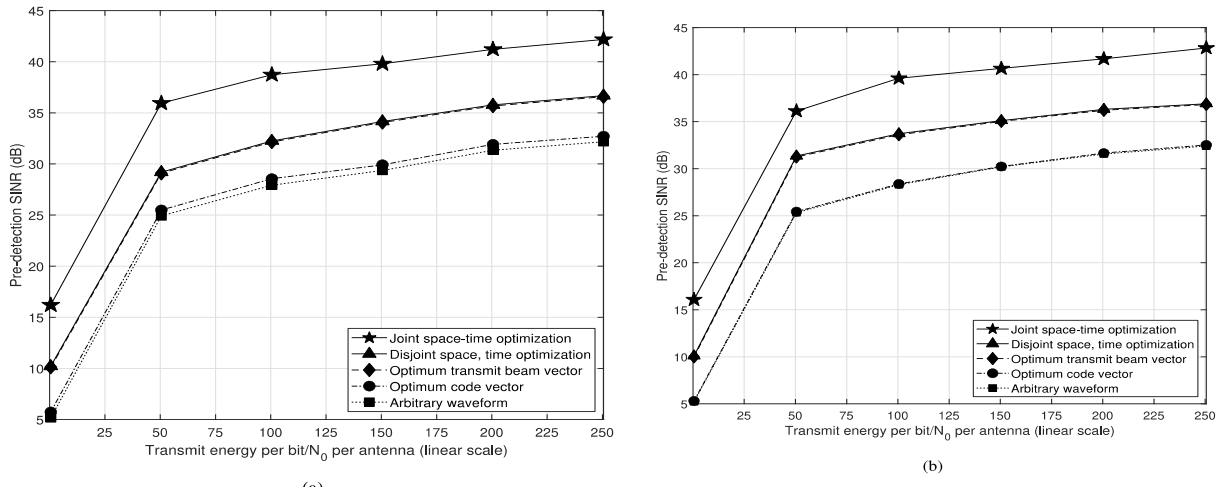

Figure 8: Pre-detection SINR in light far-field non-spread-spectrum interference ($M_t = M_r = M_{i_3} = 4$): (a) L = 4, (b) L = 16.

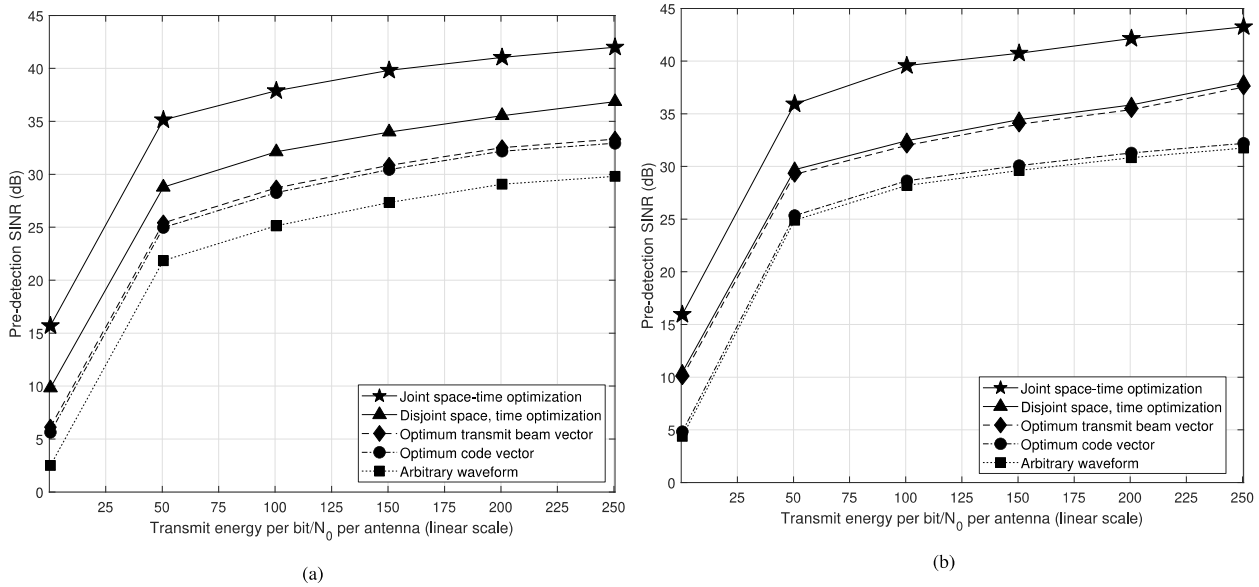

Figure 9: Pre-detection SINR in dense far-field non-spread-spectrum interference ($M_t = M_r = M_{i_3} = 4$): (a) L = 4, (b) L = 16.

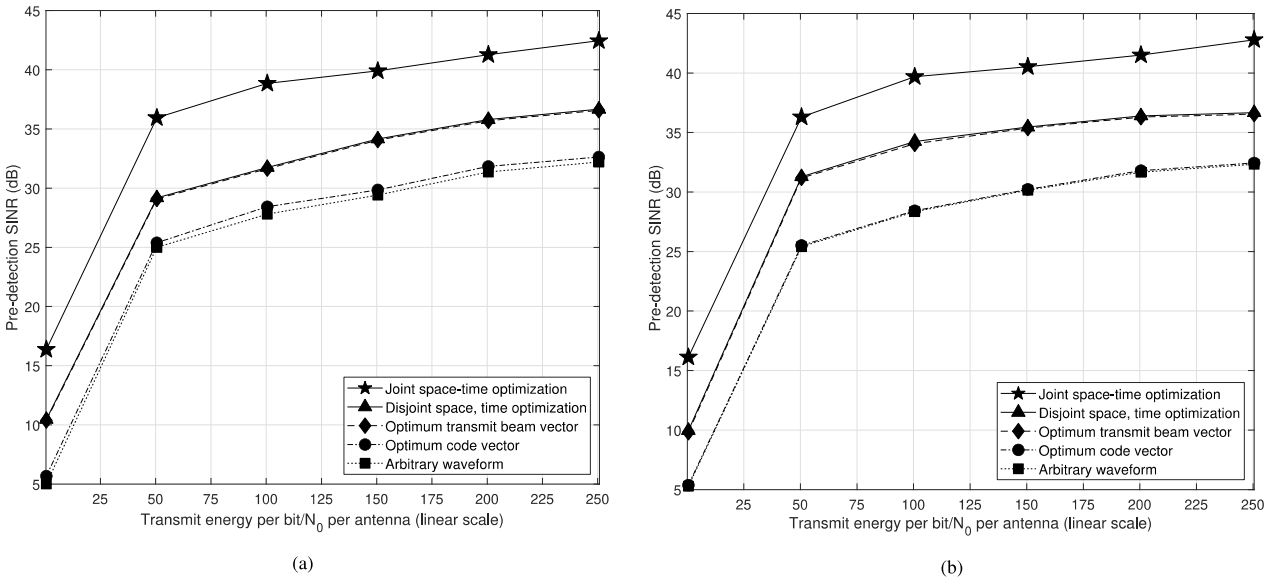

Figure 10: Pre-detection SINR in light far-field spread-spectrum interference ($M_t = M_r = M_{i_4} = 4$): (a) L = 4, (b) L = 16.

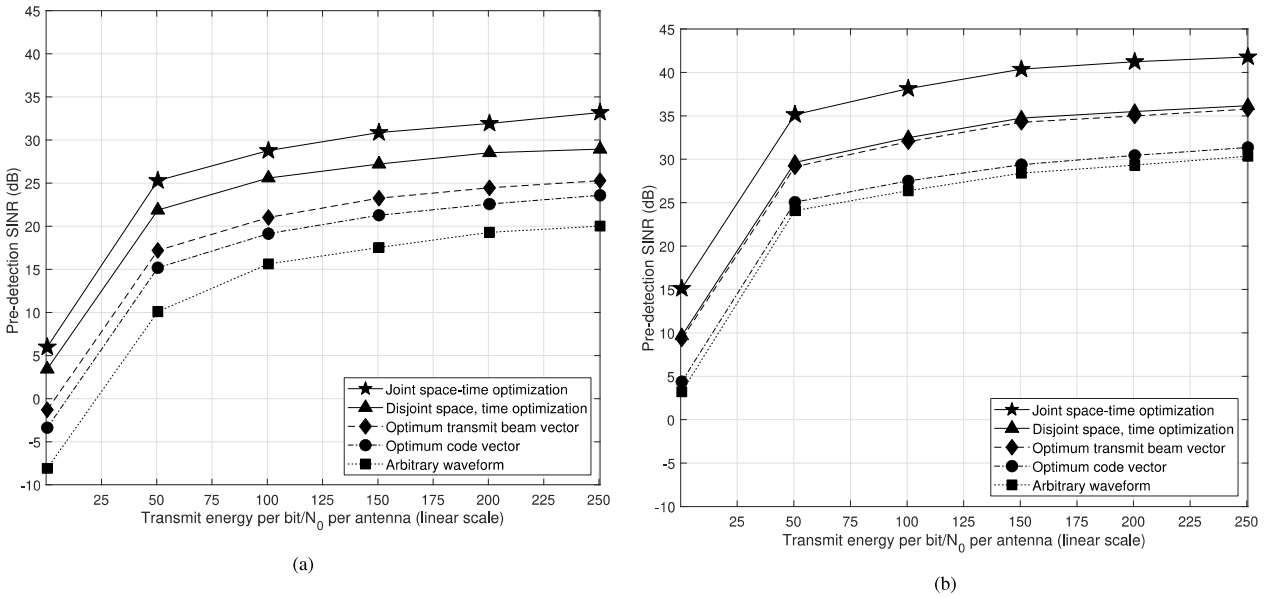

Figure 11: Pre-detection SINR in dense far-field spread-spectrum interference ($M_t = M_r = M_{i_4} = 4$): (a) L = 4, (b) L = 16.

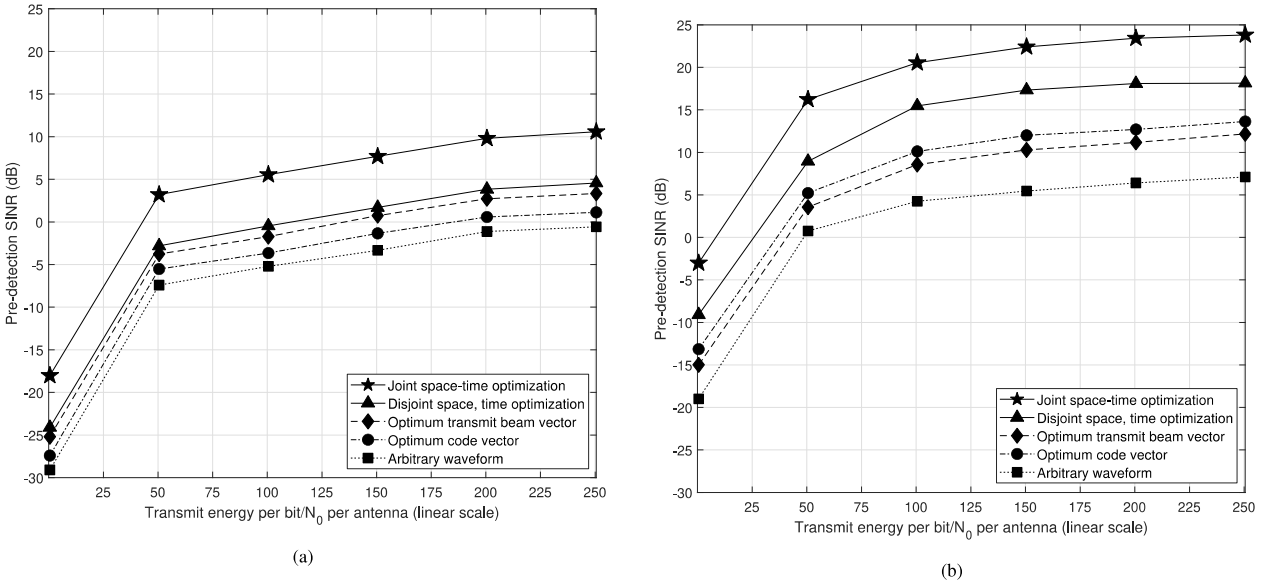

Figure 12: Pre-detection SINR in dense interference of all types ($M_t = M_r = M_{i_1} = M_{i_2} = M_{i_3} = M_{i_4} = 4$): (a) L = 4, (b) L = 16.

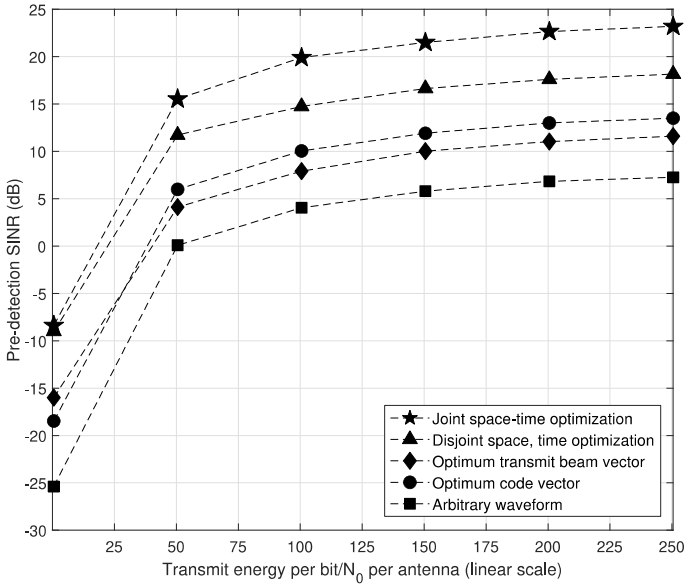

Figure 13: Pre-detection SINR under imperfect channel knowledge in dense interference of all types ($M_t = M_r = M_{i_1} = M_{i_2} = M_{i_3} = M_{i_4} = 4$): (a) L = 4, (b) L = 16.

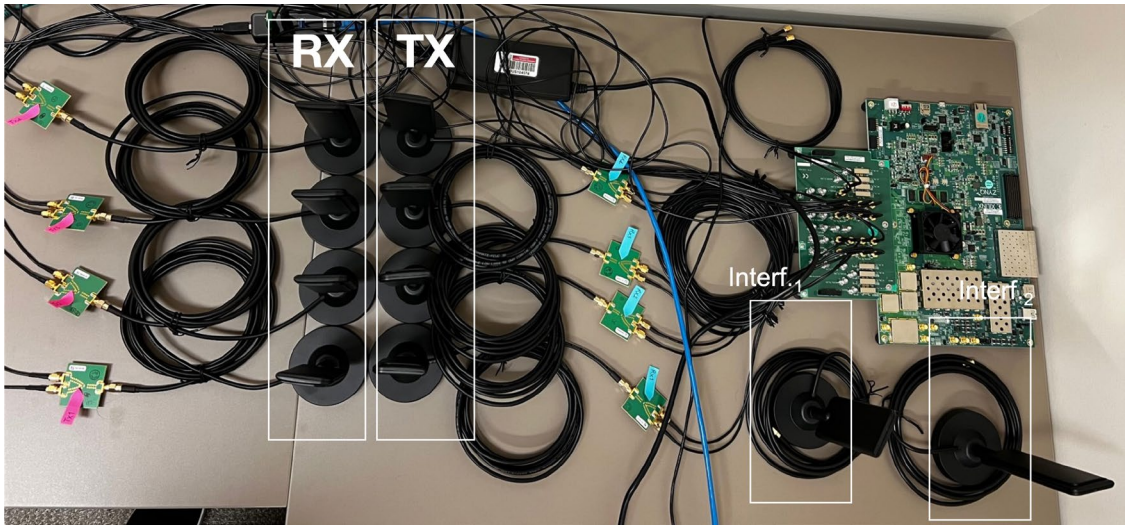

Figure 14: 4x4 RFSoC-based transceiver and two single-antenna interferers over-the-air experimental setup.

7 RF System-on-a-Chip Hardware Transceiver Design

In this section, we present a 4x4 MIMO spread-spectrum wireless link implemented on the AMD/Xilinx Zynq Ultrascale RFSoC ZCU111 evaluation board. We demonstrate interference-avoidance in the presence of either narrowband or wideband co-channel interferers. More specifically, we consider spread-spectrum transmissions in either beamforming (i.e., control the transmit beam weights with appropriate phase and gain at each antenna to maximize the signal energy at the receiver input) or diversity mode (i.e., transmitting the same data through multiple antennas to multiple receiving antennas), in the presence of interference generated from two single-antenna transmitters that are operating at the same frequency at the same time with the MIMO link of interest. At the receiver, we demonstrate the beamforming response, error vector magnitude (EVM), and received constellation after either conventional matched filtering or adaptive max-SINR space-time filtering. Link monitors and link parameters can be tuned through a standalone custom-built app during runtime. Link parameters and monitors include carrier frequency and phase offset estimation and compensation, three algorithms for timing phase offset estimation and recovery, automatic gain control (AGC) and code adaptation. Figure 14 depicts the experimental setup of the 4x4 MIMO transceiver, and the two single-antenna interferers controlled by a single RFSoC board.

Figure 15 depicts the transmit processing chain of the MIMO RFSoC-based transceiver that includes cyclic-redundancy-check (CRC) calculation, scrambling, quadrature amplitude modulation (QAM), code-waveform modulation, chip oversampling, pulse shaping, and beam-steering. The information data source generates binary information bits at a rate $R_b = 1/T_b$, where T_b is the bit interval. The information bits are mapped onto complex-valued symbols drawn from a W-point alphabet $\mathcal{A}$ at the rate $R_{sym} = 1/T_{sym} = R_b/\log_2 W$, in which T_{sym} is the symbol interval. A finite state Moore machine governs the packetization process by enabling, resetting, and controlling the counters, look-up-tables (LUTs), and valid signals throughout the transmission chain. $\log_2 W$ individual bits are concatenated into one unsigned integer for symbol mapping. The symbol mapper is a rectangular 16-QAM modulator that maps the incoming integers onto complex symbols using a Gray mapping scheme. Subsequently, each symbol is modulated into $L = 4$ chips using the spreading code $\mathbf{c} = \frac{1}{\sqrt{L}}\{\pm 1, \pm j\}^L$. The transmit square-root-raised-cosine (SRRC) filter is a finite-impulse-response (FIR) interpolation filter that oversamples and shapes the incoming chips with roll-off (or excess-

bandwidth) factor α (with $0 \leq \alpha \leq 1$), chip rate R_c, and chip duration T_c, where chip (or channel symbol) refers to the symbol interval of the spreading sequence. The bandwidth occupancy of the baseband spread-spectrum signal with SRRC shaping is $B_{\max} = (1+\alpha).R_c\ /\ 2 = (1+\alpha)\ /\ (2T_c)$ while the -3 dB bandwidth is $B_{-3\text{dB}} = R_c\ /\ 2 = 1\ /\ (2T_c)$. Spread-spectrum signals exhibit intrinsic anti-jam capability at the receiver which is directly proportional to the ratio of chip rate to bit rate known as the processing gain, $G_p = R_c\ /\ R_b = L\ /\ \log_2 W$. We demonstrate channel bandwidths of 80 MHz using a sampling rate of 122.88 Megasamples-per-sec.

Figure 15 also depicts the receiver processing chain of the MIMO RFSoC-based transceiver that includes pulse-matched filtering, frame detection, direction-of-arrival estimation, adaptive space-time max-SINR filtering, carrier frequency recovery, timing recovery, automatic gain control, symbol de-mapping, de-scrambling, CRC check and extraction of payload bits, error-vector-magnitude estimation, and BER estimation.

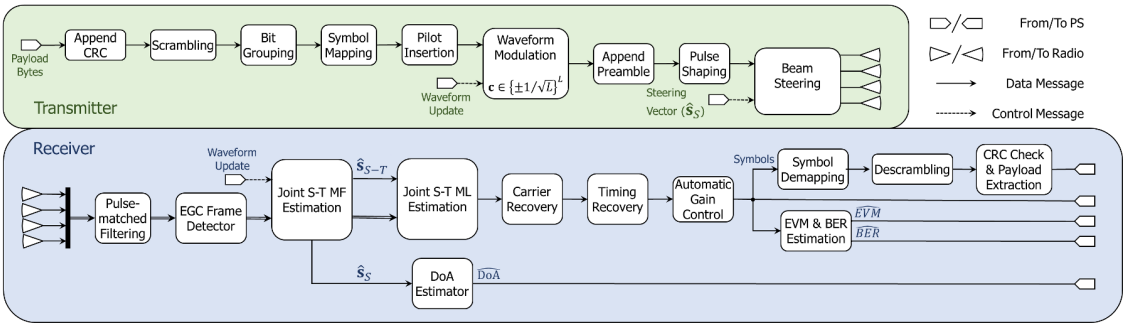

Figure 15: Top-level hardware architecture.

We set up one RFSoC board with four transmit and four receive channels and two single-antenna interferers as shown in Fig. 14. Users can select a range of transceiver configurations such as beamforming and diversity mode, link parameters such as beam-steering angle and gain for the link of interest and interferers and choose the modulation and channel bandwidth of the interfering signals from a menu including 20 MHz GMSK, 20 MHz QPSK, and 80 MHz spread-spectrum 16-QAM transmitters. Users can monitor the link quality and impact of co-channel interference by observing the variations in error vector magnitude and the received constellation diagram of the information symbols in real time using a custom-built app that is depicted in Fig. 16. We demonstrated how the link quality and beamforming response are affected by switching between matched filtering and adaptive space-time max-SINR filtering as well as manually tuning the code sequence, gain, and transmit angle-of-departure for the link of interest and the two interferers.

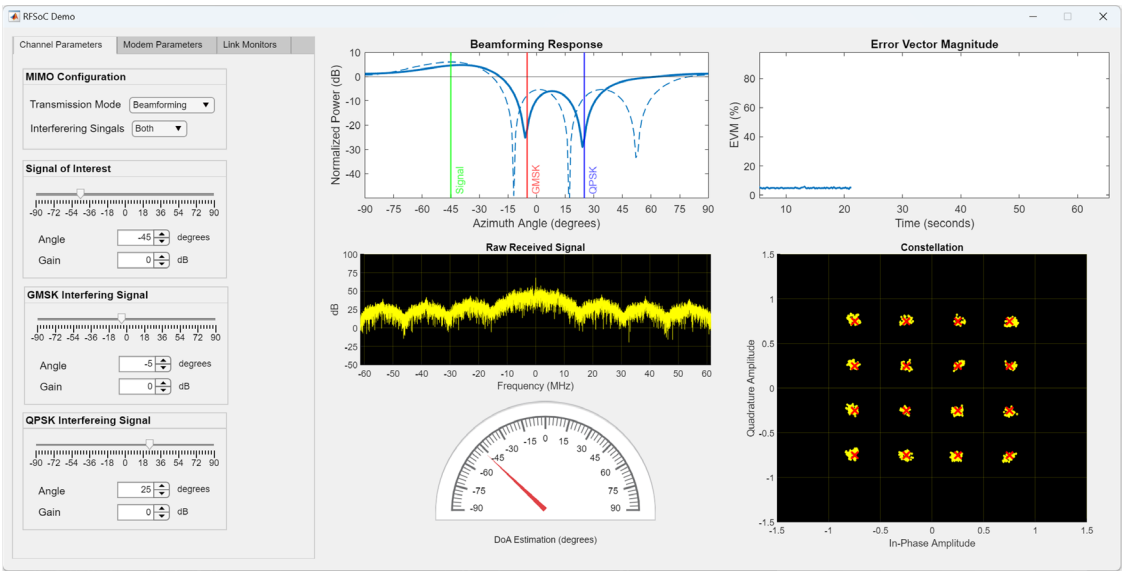

Figure 16: Host machine standalone application.

8 Conclusions

We addressed the challenge of creating a dynamic near-field or far-field MIMO wireless link over a fixed frequency band that may be heavily utilized with application focus autonomous interference-avoiding machine-to-machine communications. In particular, given a running local estimate of the disturbance autocorrelation matrix and the MIMO channel matrix coefficients, we found the optimal transmit beam weight vector and time-domain pulse code that maximize the output SINR of the maximum-SINR joint space-time receiver filter. We proposed and described in implementation detail two algorithmic solutions. The first solution carries out disjoint space-first (transmit beam weight vector) time-next (pulse code sequence) waveform optimization. The second solution succeeds in carrying out jointly optimal transmit beam weight vector and pulse code sequence optimization leaning on the closed-form expression of the optimal transmit beam vector that we derived as a function of the pulse code sequence. Notably, under joint beam weight and code vector optimization the maximum SINR space-time receiver filter simplifies to space-time matched-filtering reception.

Through extensive simulations studies, we evaluated the effectiveness of the methods in the presence of near-field/far-field, spread-spectrum/non-spread spectrum interference, in both light and dense interference scenarios. The studies highlighted the ability of the optimized waveforms, particularly joint space-time optimization, to maintain “clean" communications in extreme mixed-interference environments (i.e., attained pre-detection SINR of $15dB$ or better.)

References

[1] M. U. A. Siddiqui, F. Qamar, F. Ahmed, Q. N. Nguyen, and R. Hassan, "Interference management in 5G and beyond network: Requirements, challenges and future directions," *IEEE Access*, vol. 9, pp. 68 932–68 965, Apr. 2021.

[2] Y.Cao,T.Jiang,andZ.Han,"AsurveyofemergingM2Msystems:Context,task,andobjective,"*IEEEInternetofThings Journal*, vol. 3, pp. 1246–1258, June 2016.

[3] H. Han, Y. Li, W. Zhai, and L. Qian, "A grant-free random access scheme for M2M communication in massive MIMO systems," *IEEE Internet of Things Journal*, vol. 7, pp. 3602–3613, Apr. 2020.

[4] Z. Chen and D. Smith, "MmWave M2M networks: Improving delay performance of relaying," *IEEE Trans. on Wireless Comm.*, vol. 20, pp. 577–589, Jan. 2021.

[5] L. Chettri and R. Bera, "A comprehensive survey on internet of things (IoT) toward 5G wireless systems," *IEEE Internet of Things Journal*, vol. 7, pp. 16–32, Jan. 2020.

[6] S. Naderi, D. B. d. Costa, and H. Arslan, "Channel randomness-based adaptive cyclic prefix selection for secure ofdm system," *IEEE Wireless Comm. Letters*, vol. 11, pp. 1220–1224, June 2022.

[7] S. Naderi, D. B. da Costa, and H. Arslan, "Joint random subcarrier selection and channel-based artificial signal design aided PLS," *IEEE Wireless Comm. Letters*, vol. 9, pp. 976–980, July 2020.

[8] H. Salman, S. Naderi, and H. Arslan, "Channel-dependent code allocation for downlink mc-cdma system aided physical layer security," in *Proc. IEEE VTC*, Helsinki, Finland, Jun. 2022, pp. 1–5.

[9] Z. Li, M. A. Uusitalo, H. Shariatmadari, and B. Singh, "5G URLLC: Design challenges and system concepts," in *Proc. IEEE ISWCS*, Lisbon, Portugal, Aug. 2018, pp. 1–6.

[10] K. Zhang, X. Xu, J. Zhang, B. Zhang, X. Tao, and Y. Zhang, "Dynamic multiconnectivity based joint scheduling of eMBB and URLLC in 5G networks," *IEEE Systems Journal*, vol. 15, pp. 1333–1343, Mar. 2021.

[11] P. Popovski, K. F. Trillingsgaard, O. Simeone, and G. Durisi, "5G wireless network slicing for eMBB, URLLC, and mMTC: A communication-theoretic view," *IEEE Access*, vol. 6, pp. 55 765–55 779, Sep. 2018.

[12] S. Das and H. Viswanathan, "Interference mitigation through interference avoidance," in *Proc. Asilomar*, Pacific Grove, CA, Oct. 2006, pp. 1815–1819.

[13] C. Rose, S. Ulukus, and R. Yates, "Wireless systems and interference avoidance," *IEEE Trans. on Wireless Comm.*, vol. 1, pp. 415–428, July 2002.

[14] G. Sklivanitis, E. Demirors, A. M. Gannon, S. N. Batalama, D. A. Pados, and T. Melodia, "All-spectrum cognitive channelization around narrowband and wideband primary stations," in *Proc. IEEE GLOBECOM*, San Diego, CA, Dec. 2015, pp. 1–7.

[15] G. Sklivanitis, A. Gannon, K. Tountas, D. A. Pados, S. N. Batalama, S. Reichhart, M. Medley, N. Thawdar, U. Lee, J. D. Matyjas, S. Pudlewski, A. Drozd, A. Amanna, F. Latus, Z. Goldsmith, and D. Diaz, "Airborne cognitive networking: Design, development, and deployment," *IEEE Access*, vol. 6, pp. 47 217–47 239, July 2018.

[16] K. Tountas, G. Sklivanitis, D. A. Pados, and S. N. Batalama, "All-spectrum digital waveform design via bit flipping," in *Proc. IEEE GLOBECOM*, Abu Dhabi, UAE, Dec. 2018, pp. 1–6.

[17] L.Ding,K.Gao,T.Melodia,S.N.Batalama,D.A.Pados,andJ.D.Matyjas,"All-spectrumcognitivenetworkingthrough joint distributed channelization and routing," *IEEE Trans. on Wireless Comm.*, vol. 12, pp. 5394–5405, Nov. 2013.

[18] G. Sklivanitis, P. P. Markopoulos, S. N. Batalama, and D. A. Pados, "Sparse waveform design for all-spectrum channelization," in *Proc. IEEE ICASSP*, New Orleans, LA, Mar. 2017, pp. 3764–3768.

[19] K. Tountas, G. Sklivanitis, and D. A. Pados, "Directional space-time waveform design for interference-avoiding MIMO configurations," in *Proc. iWAT*, Miami, FL, Mar. 2019, pp. 235–238.

[20] K. Tountas, G. Sklivanitis, and D. A. Pados, "Dynamic joint PHY-MAC waveform design for IoT connectivity," in *Proc. IEEE ICASSP*, Brighton, UK, May 2019, pp. 8399–8403.

[21] J. Molins-Benlliure, E. Antonino-Daviu, M. Cabedo-Fabre´s, and M. Ferrando-Bataller, "Design of a MIMO 5G indoor base station antenna using unit cells," in *Proc. EuCAP*, Madrid, Spain, Mar. 2022, pp. 1–4.

[22] J. Zhang, E. Bjornson, M. Matthaiou, D. W. K. Ng, H. Yang, and D. J. Love, "Prospective multiple antenna technologies for beyond 5G," *IEEE Journal on Selected Areas in Comm.*, vol. 38, pp. 1637–1660, Aug. 2020.

[23] S. Mazokha, S. Naderi, G. I. Orfanidis, G. Sklivanitis, D. A. Pados, and J. O. Hallstrom, "Single-sample direction-of- arrival estimation for fast and robust 3D localization with real measurements from a massive mimo system," in *Proc. IEEE ICASSP*, Rhodes Island, Greece, Jun. 2023, pp. 1–5.

[24] Y. Takano, H.-J. Su, Y. Shiraishi, and M. Morii, "A spatial–temporal subspace-based compressive channel estimation technique in unknown interference MIMO channels," *IEEE Trans. on Signal Processing*, vol. 68, pp. 300–313, Dec. 2020.

[25] Y. Abdulkadir, O. Simpson, N. Nwanekezie, and Y. Sun, "Space-time opportunistic interference alignment in cognitive radio networks," in *Proc. IEEE WCNC*, Doha, Qatar, Apr. 2016, pp. 1–6.

[26] R. A. Osman, S. N. Saleh, and Y. N. M. Saleh, "A novel interference avoidance based on a distributed deep learning model for 5G-enabled IoT," *Sensors*, vol. 21, Sep. 2021.

[27] X. Zhao, X. Zhang, S. Li, F. Jiang, and J. Peng, "A cooperative interference eliminated mechanism in MIMO systems," in *Proc. IEEE BigComp*, Shanghai, China, Jan. 2018, pp. 569–572.

[28] S. Loyka, "On optimal signaling over Gaussian MIMO channels under interference constraints," in *Proc. IEEE GlobalSIP*, Montreal, QC, Canada, Nov. 2017, pp. 220–223.

[29] S. Loyka, "The capacity and optimal signaling for Gaussian MIMO channels under interference constraints," *IEEE Trans. on Comm.*, vol. 68, pp. 3386–3400, June 2020.

[30] M. Newinger and W. Utschick, "Interference shaping for sum-rate maximization in cellular full-duplex MIMO networks," in *Proc. IEEE GLOBECOM*, Singapore, Dec. 2017, pp. 1–6.

[31] Z. He, X. Huang, J. Zhong, and Y. Rong, "Transceiver design for interference MIMO relay systems with direct links," *IEEE Trans. on Vehicular Technology*, vol. 66, pp. 4476–4481, May 2017.

[32] E. Bjornson, O. T. Demir, and L. Sanguinetti, "A primer on near field beamforming for arrays and reconfigurable intelligent surfaces," in *Proc. Asilomar Conf. on Signals, Syst., and Comp.*, Pacific Grove, CA, Oct. 2021, pp. 105–112.

Appendix A

We consider the gradient of the objective function in (22) with respect to $\mathbf{w}_{M_t}^H$. We expand the l_2-norm and apply the hermitian operator to all components inside the first parenthesis,

$$\begin{aligned} \nabla_{\mathbf{w}_{M_t}^H} ||\mathbf{q}_{s-t} - (\mathbf{s} \otimes \mathbf{H}^T)\mathbf{w}_{M_t}||^2 = \\ \nabla_{\mathbf{w}_{M_t}^H} \left[\left(\mathbf{q}_{s-t} - (\mathbf{s} \otimes \mathbf{H}^T)\mathbf{w}_{M_t}\right)^H \left(\mathbf{q}_{s-t} - (\mathbf{s} \otimes \mathbf{H}^T)\mathbf{w}_{M_t}\right) \right] = \end{aligned} \tag{31}$$

$$\nabla_{\mathbf{w}_{M_t}^H} \left[\left(\mathbf{q}_{s-t}^H - \mathbf{w}_{M_t}^H (\mathbf{s}^T \otimes \mathbf{H}^*)\right) \left(\mathbf{q}_{s-t} - (\mathbf{s} \otimes \mathbf{H}^T)\mathbf{w}_{M_t}\right) \right]. \tag{32}$$

We set the gradient equal to $\mathbf{0} \in \mathbb{C}^{M_t}$ and calculate

$$-(\mathbf{s}^T \otimes \mathbf{H}^*)\mathbf{q}_{s-t} + (\mathbf{s}^T \otimes \mathbf{H}^*)(\mathbf{s} \otimes \mathbf{H}^T)\mathbf{w}_{M_t} = \mathbf{0}_{M_t \times 1}. \tag{33}$$

We solve (33) to obtain

$$\mathbf{w}_{M_t}^{opt} = inv[(\mathbf{s}^T \otimes \mathbf{H}^*)(\mathbf{s} \otimes \mathbf{H}^T)](\mathbf{s}^T \otimes \mathbf{H}^*)\mathbf{q}_{s-t} \tag{34}$$

where $(\mathbf{s}^T \otimes \mathbf{H}^*)(\mathbf{s} \otimes \mathbf{H}^T)$ is invertible if $rank(\mathbf{H}) \geq M_t$.

List of Abbreviations, Acronyms, and Symbols

AFRL	Air Force Research Laboratory
AGC	Automatic Gain Control
AI	Artificial Intelligence
AOA	Angle of Arrival
BER	Bit Error Rate
CRC	Cyclic Redundancy Check
DoD	Department of Defense
DOF	Degrees of Freedom
EMBB	Enhanced Mobile Broadband
EVM	Error Vector Magnitude
FAU	Florida Atlantic University
FIR	Finite Impulse Response
FPGA	Field Programmable Gate Array
GMSK	Gaussian Minimum Shift Keying
HORNets	Heterogeneous Operationally Responsive Networks
IOT	Internet of Things
KKT	Karush-Kuhn-Tucker
LUT	Look Up Table
MF	Matched Filter
MIMO	Multiple Input Multiple Output
MMTC	Massive Machine Type Communications
MM-WAVE	Millimeter wave
PI	Principal Investigator
QAM	Quadrature Amplitude Modulation

QPSK	Quadrature Phase Shift Keying
RFSOC	RF System-on-a-Chip
SINR	Signal to Interference Plus Noise Ratio
SRRC	Square Root Raised Cosine
THz	Terahertz
URLLC	Ultra Reliable Low Latency Communications